

## CHAPTER 5

### MEASUREMENT OF THE $^{55}\text{Mn}(n,\gamma)^{56}\text{Mn}$ REACTION CROSS-SECTIONS USING ACTIVATION TECHNIQUE

#### 5.1 Introduction

#### 5.2 Experimental details

#### 5.3 $\gamma$ -ray spectroscopy

#### 5.4 Calculation of neutron energy

#### 5.5 Calculation of neutron flux

#### 5.6 Calculation of the $^{55}\text{Mn}(n,\gamma)^{56}\text{Mn}$ reaction cross-sections

#### 5.7 Result and discussion

#### 5.8 Conclusion

#### References

#### **Publication related to this chapter**

Vibha Vansola, Surjit Mukherjee, Haladhara Naik, Saraswatula Venkata Suryanarayana, Reetuparna Ghosh, Sylvia Badwar, Bioletty Mary Lawriniang, Yerranguntla Santhi Sheela  
Determination of  $^{55}\text{Mn}(n, \gamma)^{56}\text{Mn}$  reaction cross-section at the neutron energies of 1.12, 2.12, 3.12 and 4.12 MeV

**Radiochimica Acta 104 (11), 749 (2016).**

## 5.1 Introduction

Manganese is a component of different steel alloys to be used for making structural and shielding materials in a reactor due to its hardenability, deoxidizer and sulphide former properties. During the operation of a reactor, the neutrons coming from the beam, interacts with Manganese present in the structural and shielding materials. Manganese has only one stable isotope  $^{55}\text{Mn}$ , which is 100% abundant in nature. When fast neutrons interact with the  $^{55}\text{Mn}$ , it forms the unstable compound nucleus  $^{56}\text{Mn}^*$ , which undergoes  $\beta^-$  decay (100%).  $^{56}\text{Mn}$  has a half-life of 2.5789 hours, which decay to stable  $^{56}\text{Fe}$  with the emission of 846.8 keV  $\gamma$ -rays. In any conventional reactor, the neutron spectrum varies from thermal to 15~20 MeV. Thus it is quite important to know the cross-sections of  $^{55}\text{Mn}(n,\gamma)^{56}\text{Mn}$  reaction at different neutron energies, which will further help us understanding the nuclear reaction mechanisms more clearly [1-11].

Literature survey shows that  $^{55}\text{Mn}(n,\gamma)^{56}\text{Mn}$  reaction cross-sections are available up to 4 MeV neutron energies and around 13.4 to 15 MeV [12-30]. From 0.97 to 19.4 MeV neutron energy range, only one data set is reported by Menlove et al. [19]. Vast discrepancies can be seen in the available literature below 4 MeV neutron energies from various authors [16-30]. Thus, there is a strong need of a reliable data set around this energy range as well as at higher incident neutron energies too. In this context,  $^{55}\text{Mn}(n,\gamma)^{56}\text{Mn}$  reaction cross-sections have been measured using the neutron activation technique. The data collection was done using the off line  $\gamma$ -ray spectroscopic technique. The  $^{55}\text{Mn}(n,\gamma)^{56}\text{Mn}$  reaction cross-sections were also compared with the theoretical nuclear reaction model codes TALYS 1.6 [31] and EMPIRE 3.2.2 [32]. Both the experimental and theoretical results were compared with the existing literature data taken from the EXFOR [12] library.

## 5.2 Experimental details

Among the four irradiations, two irradiations by using the neutron energies of 1.12 and 2.12 MeV were carried out by using FOTIA (Folded Tandem Ion beam Accelerator) facility at Nuclear Physics Division in BARC, Mumbai.  $^7\text{Li}(p,n)^7\text{Be}$  reaction was used to generate the neutron beam energies of 1.12 and 2.12 MeV with the proton beam energies of 3 and 4 MeV, respectively. A circular pellet of Lithium Fluoride (LiF) having 1 cm of diameter and 3 mm of thickness was made by using the LiF powder. It was used in the place of lithium metal foil for the production of neutrons. It was stuck on a holder at  $0^\circ$  angle relative to the exit window of the beam. In order to focus the beam, a collimator having 10 mm of diameter was used before the target. Lithium Fluoride pellet is sufficient to stop the 3 and 4 MeV proton beam.

$((\text{MnSO}_4) \cdot 2\text{H}_2\text{O})$  powder was wrapped in aluminium foils. The sample weight of this  $((\text{MnSO}_4) \cdot 2\text{H}_2\text{O})$  powder for 1.12 MeV neutron energy was 0.0735 gm and for 2.12 MeV, it was 0.0973 gm. 1 mm thick natural indium metal foils of the same size as the manganese targets, wrapped separately with the help of 0.025 mm thick super pure aluminium foil, were kept with the manganese samples. The weight of the aluminium foil in which samples were wrapped, was noted first. After taking the note of the aluminium foil, weighing was again done along with the aluminium wrapper of the target. The subtraction of the Al foil from the weight of the samples wrapped in aluminium foil gave the sample weight. The aluminium wrapped  $((\text{MnSO}_4) \cdot 2\text{H}_2\text{O})$  powder and indium metal stacks were of a square shape with 1.0  $\text{cm}^2$  size. Thus weights and sizes of both the samples are taken care of in order to minimize the size effects. These manganese and indium (In) samples were mounted one by one at  $0^\circ$  with respect to the beam direction at 3 mm distance, behind the LiF pellet. The In sample was used as a monitor to estimate the neutron flux (number of the neutrons coming from the beam to the target per unit area per unit time). A schematic arrangement of the irradiation facility carried out using FOTIA facility is given in figure 2.1 in chapter 2.

The samples were irradiated for 8 hours 32 minutes with the proton energy of 3 MeV and for 7 hours 45 minutes with proton energy 4 MeV. The incident beam current during both the irradiations of 3 and 4 MeV proton energy was kept at constant 100 nA. All the activated samples were cooled for 1 to 2 hours. After the cooling, samples were detached carefully with the use of forceps from the holder stand and kept inside a lead pot and brought to counting room. All the samples are then mounted on different Perspex plates and kept in front of an HPGe detector for  $\gamma$ -ray counting [33].

In the second set of experiment, 14UD Pelletron facility at BARC-TIFR (Bhabha Atomic Research Centre - Tata Institute of Fundamental Research), Mumbai, India has been used to irradiate the samples with 3.12 MeV and 4.12 MeV neutron energies. This has been done since the accelerator in FOTIA (BARC) is able to deliver accurately, the proton beams only up to 6 MeV energy [33]. On the other hand, in BARC-TIFR Pelletron facility, the proton energy can be up to 24 MeV based on the terminal voltage of 12 MV. Here, again, the desired neutron beams were obtained from the  ${}^7\text{Li}(p,n){}^7\text{Be}$  reaction, as mentioned above, using proton beams of 5 and 6 MeV in the main line, 6 m above the analysing magnet of the Pelletron. The 6 meter port was used to utilize the maximum proton current from the Pelletron. The broadening of proton beam at 6 meter port was found to be around 50~90 keV. A terminal potential stabilizer was used in order to regulate the terminal voltage by

generating the voltage mode (GVM). A collimator having 6-mm diameter was used before the target to get circular shaped beam. The lithium metal foil having  $3.7 \text{ mg/cm}^2$  thickness was placed in between two tantalum foils having different thicknesses. The thinnest tantalum foil of thickness  $3.9 \text{ mg/cm}^2$  faces the proton beam (front tantalum). The degradation of the proton energy in the front Ta foil was estimated by using the SRIM code [34] and was found to be around 30 keV. In order to stop the proton beam, the thickness of the back tantalum foil was kept  $6.66 \text{ mg/cm}^2$  (0.025 mm). Specific amount of  $\text{MnO}_2$  manganese oxide powder was wrapped in the super pure aluminium foil. The sample ( $\text{MnO}_2$  powder) weights were 0.0657 gm and 0.0166 gm for 3.12 and 4.12 MeV neutron energies, respectively. These manganese samples were wrapped in 0.025 mm thick super pure aluminium foil. Similarly, 1 mm thick natural indium metal foils were also wrapped separately in 0.025 mm thick super pure aluminium foil. Both the manganese and indium metal foils were now again packed in a common aluminium foil. Sizes of both the samples were kept the same in order to avoid the size effect. The size of  $\text{MnO}_2$  powder sample wrapped in aluminium foil was  $1.0 \text{ cm}^2$  and the thickness was  $29.3 \text{ mg/cm}^2$ . They were wrapped with Al foils separately so that the reaction products can be stopped from recoiling out from the surface of the samples and collected easily. Two different sets of manganese and indium were prepared for two different irradiations for the neutron energies of 3.12 and 4.12 MeV, respectively. With these two different aluminium foils, the individual stacks of aluminium wrapped  $\text{MnO}_2$  powder and aluminium wrapped indium metal samples were additionally prepared. As described in reference [33], samples were mounted behind the Ta–Li–Ta stack at a distance 2.1 cm and at an angle of  $0^\circ$  with respect to the beam direction. A schematic arrangement of the irradiation facility carried out using Pelletron accelerator facility is given in figure 2.2 in chapter 2.

Proton beam with energies 5 and 6 MeV were bombarded on Ta–Li–Ta stack. One set of samples was irradiated with 3.12 MeV neutron energy for 13 h 25 min and the other set of samples was irradiated with 4.12 MeV neutron energy for 11 h 50 min. For both the experiments, the proton current was around 60~70 nA. Activated samples were cooled for 2 hours 30 minutes and 2 hours 9 minutes, respectively. After cooling the samples, they were mounted on different Perspex plates with the help of a forceps and kept in front of the HPGe detector for  $\gamma$ -ray counting.

### 5.3 $\gamma$ -ray spectroscopy

The  $\gamma$ -ray counting was done with the help of energy and efficiency calibrated  $80 \text{ cm}^3$  HPGe detector (High Purity Germanium detector). The HPGe detector was coupled to a

personal computer system based 4K multi-channel analyser (MCA). To avoid pile-up effects, activated samples were kept at significant distance from the detector window so that the dead time of a detector will be less than 5 %. The energy and efficiency calibration of the HPGe detector was done using the  $\gamma$ -ray energies of a standard source,  $^{152}\text{Eu}$ , by keeping the same geometry, where summation error was almost zero. This was checked by comparing the efficiency using other standard sources like  $^{241}\text{Am}$  (59.5 keV),  $^{133}\text{Ba}$  (80.9, 276.4, 302.9, 356.0, and 383.8 keV),  $^{137}\text{Cs}$  (661.7 keV),  $^{54}\text{Mn}$  (834.6 keV), and  $^{60}\text{Co}$  (1173 and 1332.5 keV). Relative efficiency of the HPGe detector was 20 % at 1332.5 keV  $\gamma$ -ray energy, with respect to the 73.5 mm diameter and 73.5 mm long NaI(Tl) detector. In this efficiency, the uncertainty was found to be 2–3 %. The resolution of the HPGe detector had a FWHM (full-width at half-maximum) of 1.8 keV for  $^{60}\text{Co}$ , at  $\gamma$ -ray energy of 1332.5 keV. The  $\gamma$ -ray counting of the activated Mn and In samples were done at least for three half-lives for the minimization of error associated with the peak area, in the calculation of the cross-section.

**Table 5.1:** Nuclear spectroscopic data of the products from the  $^{115}\text{In}(n,\gamma)^{116\text{m}}\text{In}$  and  $^{55}\text{Mn}(n,\gamma)^{56}\text{Mn}$  reactions used in the calculation from Ref. [38]

Nuclide	Spin-Parity	Half life	Decay Mode	$\gamma$ -Energy (keV)	$\gamma$ -Abundance (%)
$^{116\text{m}}_{49}\text{In}$	8-	2.18±4sec	IT:100%	138.33	3.7
				416.86	27.2
				818.72	12.13
				1097.33	58.5
				1293.56	84.8
$^{116\text{g}}_{49}\text{In}$	5+	54.29±17min	$\beta^-$ :100%	<b>138.33</b>	<b>3.7</b>
				<b>416.86</b>	<b>27.2</b>
				<b>818.72</b>	<b>12.13</b>
				<b>1097.33</b>	<b>58.5</b>
				<b>1293.56</b>	<b>84.8</b>
$^{116\text{g}}_{49}\text{In}$	1+	14.10±3sec	$\beta^-$ :99.98% & $\epsilon$ :0.02%	138.33	3.7
				416.86	27.2
				818.72	12.13
				1097.33	58.5
				1293.56	84.8
$^{56}_{25}\text{Mn}$	3+	2.5789±1 h	$\beta^-$ :100%	<b>846.8</b>	<b>98.85</b>

#### 5.4 Calculation of the neutron energy

In order to get the desired neutron energies of 1.12, 2.12, 3.12 and 4.12 MeV, we have used the  ${}^7\text{Li}(p,n){}^7\text{Be}$  reaction. The interaction of protons of 3, 4, 5 and 6 MeV energies with the  ${}^7\text{Li}$  target produce fast neutrons. For  ${}^7\text{Li}(p,n){}^7\text{Be}$  reaction, the Q-value of the ground state is -1.644 MeV, whereas for the first excited state, it is 0.431 MeV above the ground state. This leads to the average Q-value of -1.868 MeV. The threshold value of  ${}^7\text{Li}(p,n){}^7\text{Be}$  reaction to the ground state of  ${}^7\text{Be}$  is 1.881 MeV. One has to subtract this threshold energy from the proton energy in order to get the neutron energy of a peak. Thus, the first group of neutrons ( $n_0$ ) for proton energies 3, 4, 5 and 6 MeV will have the peak energy of 1.12, 2.12, 3.12 and 4.12 MeV, respectively. For the first excited state of  ${}^7\text{Be}$ , the second group neutrons ( $n_1$ ) will have corresponding neutron energies of 0.63, 1.63, 2.63 and 4.63 MeV, respectively [35-37]. The reason behind the production of this second group of neutrons is break up of  ${}^7\text{Be}$ , above 2.37 MeV proton energy. Liskien and Paulsen [35] and Meadows and Smith [36] have given the branching ration to the ground state and first excited state of  ${}^7\text{Be}$  up to 7 MeV proton energy. The branching ratio of the proton energies from 4.2 to 26 MeV of the ground and first excited state have also been given by Poppe et al. [37]. On the basis of the description given by them [35-37], the contribution of  $n_0$  (first excited state group of neutrons) and  $n_1$  (second excited state group of neutrons) is 85% and 15%, respectively for the 6 MeV proton energy.

If there is 6 MeV proton energy beam, then the corresponding neutron energy will be the threshold energy subtracted from the proton energy. i.e.,  $6-1.881=4.12$  MeV. This is the case when we take first neutron group into consideration. Now if we take second group of neutron into consideration, we will have the neutron energy of 3.63 MeV. The average neutron energy will be  $4.12 \times 0.85 + 0.63 \times 0.15 = 4.05$  MeV. This average value falls within the uncertainty of neutron peak energy of 4.12 MeV. Hence, one can say that  $n_1$  group neutrons have some contribution on main peak. It is clear that  $n_1$  causes the broadening of the main peak. Therefore, for the proton energies of 3, 4, 5 and 6 MeV, the corresponding neutron energies will be  $1.12 \pm 0.11$ ,  $2.12 \pm 0.15$ ,  $3.12 \pm 0.21$  and  $4.12 \pm 0.32$  MeV, respectively. Above 4.5 MeV proton energy, neutron energy spectra has full energy peak because of  ${}^7\text{Li}(p,n){}^7\text{Be}$  reaction and due to multi-body break up process, continuum components are there in the spectra i.e.,  ${}^7\text{Li}(p,n^3\text{He}){}^4\text{He}$  reaction has the Q-value of -3.231 MeV. This has an impact on the continuous neutron energy distribution. Because of this impact, the distribution possesses a tail besides the  $n_0$  and  $n_1$  groups of neutrons. There is no tail part in neutron spectrum up to 5 MeV proton energy [33]. Above 6 MeV proton energy, only very small tail part is there [33], which is negligible. So it can be neglected in the

average neutron energy calculation. Similarly, it can also be neglected in the  $^{55}\text{Mn}(n,\gamma)^{56}\text{Mn}$  reaction cross-section calculation.

### 5.5 Calculation of neutron flux

In the present work, the  $^{115}\text{In}(n,\gamma)^{116\text{m}}\text{In}$  reaction cross-section has been used as the neutron flux monitor. For  $^{116\text{m}}\text{In}$ , there are several intense  $\gamma$ -ray peaks like 138.3, 416.9, 818.7, 1097.3 and 1293.6 keV. The photo-peak activities of these  $\gamma$ -lines of  $^{116\text{m}}\text{In}$  from the  $^{115}\text{In}(n,\gamma)^{116\text{m}}\text{In}$  reaction were used for the calculation of neutron flux. The spectroscopic data used in neutron flux calculation are given in the table 5.1. These data were taken from the reference [38]. In the  $\gamma$ -ray spectrum of  $^{116\text{m}}\text{In}$ , we did the Compton background subtraction from the total photo-peak areas. The photo-peak areas for the numbers of detected  $\gamma$ -rays ( $A_{\text{obs}}$ ) of  $^{116\text{m}}\text{In}$  and  $^{56}\text{Mn}$  reaction products were obtained after the subtraction the linear Compton background from the total peak areas. Hence, we get only net area under the curve, which is the activity of irradiated indium ( $A_{\text{obs}}$ ).

Table 5.1 shows that the  $^{116\text{m}}\text{In}$  has 54.29 minutes half-life which has five intense  $\gamma$  lines with good branching intensities. The photo-peak activities ( $A_{\text{obs}}$ ) of the  $^{116\text{m}}\text{In}$  at 138.33, 416.86, 818.72, 1097.33 and 1293.56 keV  $\gamma$ -lines are used to find the neutron flux ( $\phi$ ). This neutron flux was calculated by using equation (2.3) from the reference [33].

where,  $A$ =Photo-peak activity of the  $\gamma$ -ray of  $^{116\text{m}}\text{In}$

$\lambda$  = the decay constant ( $\lambda = \frac{\ln 2}{T_{1/2}}$  of the reaction product of interest with half-life,

$I_\gamma$  is the branching intensity of the 138.33, 416.86, 818.72, 1097.33 and 1293.56 keV  $\gamma$ -line of  $^{116\text{m}}\text{In}$  [38].

$\sigma_R$ = the cross-section of the  $^{115}\text{In}(n,\gamma)^{116\text{m}}\text{In}$  reaction

Half-lives and  $I_\gamma$  are taken from EXFOR site in NuDat section [12, 38].

The  $^{115}\text{In}(n,\gamma)^{116\text{m}}\text{In}$  reaction cross-section at the neutron energy of 1.96 to 7.66 MeV are available in the Refs. [30, 39-41]. It was observed that, only Husain et al. [40] has reported the data within the 2.44 to 4.5 MeV neutron energy range and are slightly higher than other authors' result [30, 39, 41]. So  $^{115}\text{In}(n,\gamma)^{116\text{m}}\text{In}$  reaction cross-sections from the Refs. [30, 39, 41] were used in calculating the neutron flux. Theoretically computed  $^{115}\text{In}(n,\gamma)^{116\text{m}}\text{In}$  reaction cross-section data as a function of neutron energy are available in the IRDFF-1.05 library [42]. Evaluated  $^{115}\text{In}(n,\gamma)^{116\text{m}}\text{In}$  reaction cross-sections ( $\sigma_s$ ) were taken from Refs. [30, 39, 41-42].

The calculated neutron flux for all the four neutron energies 1.12, 2.12, 3.12 and 4.12 MeV is given in table 5.2. These neutron flux have been used in the calculation of  $^{55}\text{Mn}(n,\gamma)^{56}\text{Mn}$  reaction cross-section.

### 5.6 Calculation of the $^{55}\text{Mn}(n,\gamma)^{56}\text{Mn}$ reaction cross-sections

For the calculation of cross-section of  $^{55}\text{Mn}(n,\gamma)^{56}\text{Mn}$  reaction  $\gamma$ -line of 846.8 keV energy from the  $\gamma$ -ray spectrum of activated  $^{56}\text{Mn}$  was used. Also the photo peak activity of 846.8 keV  $\gamma$ -ray energy along with the other neutron spectroscopic data were used. These input parameters are given in table 5.1 [38]. For the calculation of  $^{55}\text{Mn}(n,\gamma)^{56}\text{Mn}$  reaction cross-section, equation 2.20 from chapter 2 was used.

All the notations in this equation are well explained before in the equation of flux. The neutron flux  $\phi$  was taken from table 5.2 in order to calculate the  $^{55}\text{Mn}(n,\gamma)^{56}\text{Mn}$  reaction cross-section. During the operation of a reactor, the self-shielding of neutrons in the sample takes place. It should be corrected using some correction factor which is related to the sample size. After this correction only further calculation of  $^{55}\text{Mn}(n,\gamma)^{56}\text{Mn}$  reaction cross-section should be done [43-44]. Ratio of an average fluence rate inside the volume of the sample to the fluence rate incident on the sample is known as a neutron self-shielding factor [44]. Size of the sample, neutron energy spectrum inside and outside the sample, absorption as well as the scattering cross-section can treat the neutron self-shielding problem completely. For the present work, main target sample size and monitor sample size are very small. Also both the main target and flux monitor reaction cross-sections are not in the resonance region. The neutron shielding wall was far from the experimental set up, so there was no chance for neutron scattering. In addition to this, both  $^{115}\text{In}(n,\gamma)^{116\text{m}}\text{In}$  and  $^{55}\text{Mn}(n,\gamma)^{56}\text{Mn}$  excitation functions have the same nature.

If there will be any scattered neutrons with low energy present in the far surrounding wall, then their effect will be nullified because of the similar trend of reaction cross-sections of the sample and monitor. Hence, in the present work, the impact of the self shielding of neutrons for the sample size is negligible. Hence, it is neglected in the present work in the calculation of  $^{55}\text{Mn}(n,\gamma)^{56}\text{Mn}$  reaction cross-section. Different values of  $^{55}\text{Mn}(n,\gamma)^{56}\text{Mn}$  reaction cross-section using different flux are given in the table 5.2.

### 5.7 Result and discussions

As demonstrated in the above section, the  $^{55}\text{Mn}(n,\gamma)^{56}\text{Mn}$  reaction cross-sections were measured for the four different neutron energies 1.12, 2.12, 3.12 and 4.12 MeV for the very first time and are given in table 5.2. Measured  $^{55}\text{Mn}(n,\gamma)^{56}\text{Mn}$  reaction cross-section has the

uncertainty, which is the quadratic sum of both statistical and systematic errors. The estimated random error in the observed  $\gamma$ -ray activity of  $^{56}\text{Mn}$  is approximately 3.1 to 5.5 % because of the counting statistics. It can be determined by the accumulation of the data for optimum time period which depends on the half-life of the  $^{56}\text{Mn}$  nuclide. Also there are uncertainties in the irradiation time ( $\sim 0.1\%$ ), half-life of the products,  $\gamma$ -ray intensity (1%) and detector efficiency ( $\sim 3\%$ ). Error in the detector efficiency arises because of the extrapolation and fitting of the data set. All these uncertainties add up to be systematic errors in the computation. The chances of systematic error increasing drastically depend on the  $^{115}\text{In}(n,\gamma)^{116\text{m}}\text{In}$  reaction cross-section, used to find the flux and finally it reflects on the  $^{55}\text{Mn}(n,\gamma)^{56}\text{Mn}$  reaction cross-section. It adds up to be the maximum systematic error (3.8~14.4%) [30, 39-42]. Hence, the total systematic error turns out to be 4.9~14.8%. The total sum of both statistical and systematic errors falls within the range 5.8~15.8% for the  $^{55}\text{Mn}(n,\gamma)^{56}\text{Mn}$  reaction cross-section.

**Table 5.2:**  $^{115}\text{In}(n, \gamma)^{116\text{m}}\text{In}$  and  $^{55}\text{Mn}(n, \gamma)^{56}\text{Mn}$  reaction cross-sections at different neutron energies along with the neutron flux

Proton Energy (MeV)	Neutron Energy (MeV)	$^{115}_{49}\text{In}(n, \gamma)^{116\text{m}}_{49}\text{In}$ Reaction cross- section (mb)	Flux (n/cm <sup>2</sup> sec)	$^{55}_{25}\text{Mn}(n, \gamma)^{56}_{25}\text{Mn}$ reaction cross-section	
				Measured Data (mb)	TALYS- 1.6 (mb)
3	1.12	247.1±28.6 [30]	5.67099E+06	3.374±0.487	3.872
	±0.12	174.4±6.7 [42]	8.03273E+06	2.382±0.344	
4	2.12	129.0±9.1 [39]	1.29330E+07	1.563±0.147	3.031
	±0.15	104.1±4.5 [42]	1.51154E+07	2.062±0.126	
5	3.12	44.6±3.2 [41]	2.03785E+07	1.407±0.136	1.721
	±0.21	37.5±1.5 [42]	2.41184E+07	1.184±0.117	
6	4.12	16.7±2.4 [41]	7.23707E+07	1.137±0.178	1.149
	±0.32	15.7±0.7 [42]	7.72136E+07	1.066±0.167	

At 4.12 MeV, the  $^{55}\text{Mn}(n,\gamma)^{56}\text{Mn}$  reaction cross-section is measured experimentally for the first time in the literature. As per the elaborated literature survey,  $^{55}\text{Mn}(n,\gamma)^{56}\text{Mn}$  reaction cross-sections are available within 4 MeV neutron energy range and around 13.4 to 15 MeV [13-30]. Menlove et al. [19] has reported one set of data in the energy range of 0.97 to 19.4 MeV. Except the data of Menlove et al. [19], rest of all these data from Refs. [16-30] are plotted in figure 5.1.

It can be seen from figure 5.1, within neutron energies of 0.5 to 3.43 MeV, the literature data of  $^{55}\text{Mn}(n,\gamma)^{56}\text{Mn}$  reaction cross-section have three different trends. On higher side, there are data of Gautam et al. [30], whereas on the lower side, within neutron energy of 3.43 MeV there are data of Stavisskiy et al. [17], Menlove [19] and Dovbenko et al. [21]. There are data sets of Jonsurd et al. [16] and Trofimov et al. [29] those fall within the above mentioned data. The present experimental data at 1.12 and 2.12 MeV neutron energies are falling in the region of these two data sets but in close agreement with Jonsurd et al. [16] and Trafimov et al. [29] data. Present datum at 3.12 MeV is in good agreement with the data of Menlove et al. [19] and Dovbenko et al. [21]. The present datum at 4.12 MeV energy again matches well with the data of Menlove et al. [19]. Figure 3 shows that below 3.43 MeV neutron energy, three data sets given in the literature [16, 17, 19, 21, 29]. In which, there are lots of discrepancies. In accordance with this, the  $^{55}\text{Mn}(n,\gamma)^{56}\text{Mn}$  reaction cross-sections within the energy range of 1 to 20 MeV were computed theoretically using nuclear model codes TALYS [31] and EMPIRE [32]. The theoretical values from TALYS [31] and EMPIRE [32] are compared with the experimental data in figure 5.1.

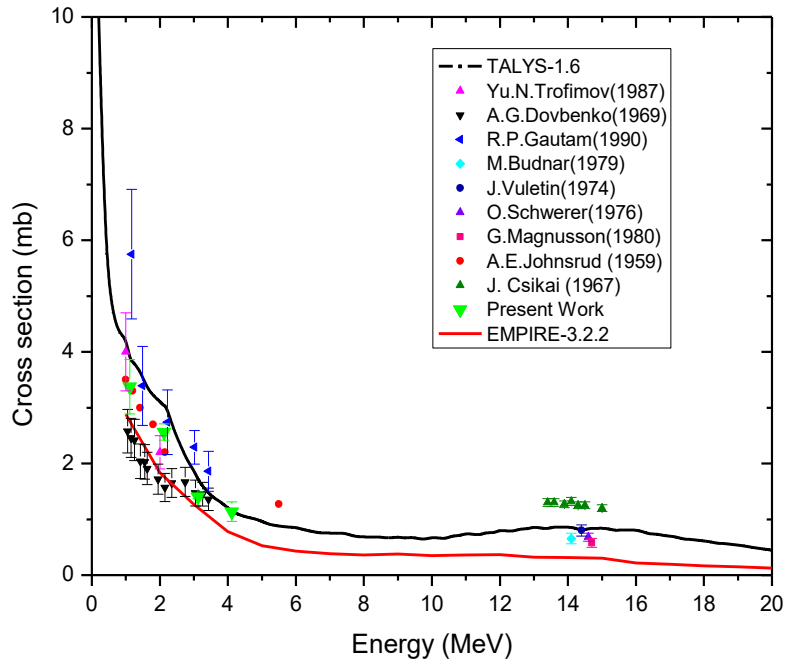


**Figure: 5.1** Comparison of experimental  $^{55}\text{Mn}(n,\gamma)^{55}\text{Mn}$  reaction cross-section from the present work and literature data [17, 19, 21, 29, 30] with the theoretical values from TALYS 1.6 [31] and EMPIRE-3.2.2 [32]

It is clear from figure 5.1 that the measured data of Gautam et al. [30] and few of Trofimov et al. [29] data are close to the theoretically evaluated data. The measured data of Stavisskiy et al. [17] Menlove et al. [19] and Dovbenko et al. [21] below 3.43 MeV are closer to the theoretical values of nuclear model code EMPIRE [32]. The measured data of Johnsurd et al. [16] and present experimental data below 3.43 MeV fall in between the theoretically computed TALYS [31] and EMPIRE [32] data. Same is the case with the 14 MeV data, the literature data around 14 MeV fall in between the theoretically computed TALYS and EMPIRE. The data of Johnsurd et al. [16] at 5.5 MeV neutron energy and Csikai et al. [18] around 13.4 to 15 MeV are greater than the theoretically computed values of TALYS [31] and EMPIRE [32]. The present data at 4.12 MeV neutron energy and the data of Menlove et al. [19] from 4 to 19.39 MeV are nearer to the theoretically computed data using TALYS [31].

## 5.8 Conclusion

At the four different neutron energies 1.12, 2.12, 3.12 and 4.12 MeV, the  $^{55}\text{Mn}(n,\gamma)^{56}\text{Mn}$  reaction cross-sections were determined by using neutron activation and off-line gamma ray spectroscopic technique. The present data at the neutron energy of 4.12 MeV was measured for the first time. The measured data at other three neutron energies are in good agreement with one set of experimentally measured data available in the literature but not with the other two sets. The  $^{55}\text{Mn}(n,\gamma)^{56}\text{Mn}$  reaction cross-sections were also computed theoretically with the use of two nuclear model codes, TALYS and EMPIRE. Both theoretical and measured data fall well within the range of available literature data.

## References:

- [1] R. K. Sinha, A. Kakodkar, Nucl. Eng. Des. **236**, 683 (2006).
- [2] T. R. Allen, D. C. Crawford, Sci. Technol. Nucl. Install. **2007**, 11 (2007).
- [3] A. Nuttin, D. Heuer, A. Billebaud, R. Brissot, C. Le Brun, E. Liatard, J. M. Loiseaux, L. Mathieu, O. Meplan, E. Merle-Lucotte, H. Nifenecker, F. Perdu, S. David, Prog. Nucl. Energy **46**, 77 (2005).
- [4] L. Mathieu, D. Heuer, R. Brissot, C. Garzenne, C. Lebrun, E. Liatard, J. M. Loiseaux, O. Meplan, E. Nuttin, Proceedings of the Global International Conference, Paper No. **428**, Tsukuba, Japan (2005).
- [5] Fast Reactors and Accelerator Driven Systems Knowledge Base, IAEA- TECDOC-1319: Thorium fuel utilization: Options and Trends (Nov. 2002).
- [6] F. Carminati, R. Klapisch, J. P. Revol, Ch. Roche, J.A. Rubia, C. Rubia, An Energy Amplifier for Cleaner and Inexhaustible Nuclear Energy Production Driven by Particle Beam Accelerator, CERN/AT/93-49 (ET) (1993).
- [7] E. D. Arthur, S. A. Schriber, A. Rodriguez (Editors), The International Conference on Accelerator- Driven Transmutation Technologies and Applications, Las Vegas, Nevada, USA, 1994, AIP Conf. Proc., **346** (1995).
- [8] C. Rubia, J. A. Rubio, S. Buono, F. Carminati, N. Fietier, J. Galvez, C. Geles, Y. Kadi, R. Klapisch, P. Mandrillon, J. P. Revol, Ch. Roche, Conceptual design of a fast neutron operated high power energy amplifier. CERN/AT/95-44 (ET) (1995).
- [9] Accelerator Driven Systems: Energy Generation and Transmutation of Nuclear Waste, Status report, IAEA, Vienna, IAEA-TECDO- 985, (1997).
- [10] C. D. Bowman, Ann. Rev. Nucl. Part Sci. **48**, 505 (1998).
- [11] S. S. Kapoor, Pramana- J.Phys **59**, 941 (2002).
- [12] N. Otsuka et al., Experimental nuclear reaction data. Nucl.Data Sheets **120**, 272 (2014).
- [13] A. I. Leipunskiy et al., Fiziko-Energeticheskii Inst., Obninsk, Russia, second UN Conf. On the Peaceful Uses of Atomic Energy. Geneva, 1-13 Sept. 15, **50**, 2219 (1958).
- [14] L. Perkin, L. P O'Connor, R. F. Coleman, Proc. Physical Soc. **72**, 505 (1958).
- [15] N. A. Bostrom, I. L. Morgan J. T. Prud'homme, P. L. Okhuysen, Jr. O. M. Hundson, radio lead and bismuth. Report No. WADC-TN-59-107 (1959).
- [16] A. E. Johnsrud, M. G. Silbert, H. H. Barschall, Phys. Rev. **116**, 927 (1959).
- [17] J. Y. Stavisskiy, V. A. Tolstikov, Atomnaya Energiya **10(5)**, 508 (1961).
- [18] J. Csikai, G. Peto, M. Buczko, Z. Milligy, N. Eissa, Nucl. Phys. **A95**, 229 (1967).
- [19] H. O. Menlove, K. L. Coop, H. A. Grench, R. Sher, Phys. Rev. **163**, 1299 (1967).

- [20] G. Peto, Z. Milligy, I. Hunyadi, J. Nul. Energ. **21**, 797 (1967).
- [21] A. G. Dovbenko, V. E. Kolesov, V. P. Koroleva, V. A. Tolstikov, Soviet Atomic Energy **26**, 82 (1969).
- [22] J. Vuletin, P. Kulisic, N. Cindro, Lettereal Nuovo Cimento **10**, 1 (1974).
- [23] O. Schwerer, M. Winklerrohatsch, H. Warhanek, G. Winkler, Nucl. Phys. A **264**, 105 (1976).
- [24] Manjushree Majumder, B. Mitra, B. Trans. Bose Research Inst., Calcutta **40(3)**, 81 (1977).
- [25] M. Budnaret al., INDC (YUG)-6 (1979).
- [26] G. Magnusson, P. Andersson, I. Berquist, Physica Scripta **21(1)**, 21(1980).
- [27] B. M. Bahal, R. Pepelnik, Ges. Kernen Verwertung, Schiffbau and Schiffahrt **E 85**, 11 (1985).
- [28] Y. N. Trofimov, Int. Conf. On Neutron Physics, Kiev, 14–18 Sep. **3**, 331 (1987).
- [29] Y. N. Trofimov, Vop. At. Naukii Tekhn., Ser. Yadernye Konstanty **4**, 10 (1987).
- [30] R. P. Gautam, R. K. Singh, I. A. Rizvi, M. Afzal Ansari, K. Chaubey, S. Kailas, Indian J. Pure Appl. Phy. **28**, 235 (1990).
- [31] A. J. Koning, S. Hilaire, M. C. Duijvestijn, TALYS-1.6, A nuclear reaction Program. NRG-1755 N G Petten, The Netherlands, <http://www.talys.eu>. (2008).
- [32] M. Herman, Empire II statistical model code for nuclear reaction calculations. IAEA, Vienna (2002).
- [33] V. Vansola et al., Radiochim. Acta **103**, 817 (2015).
- [34] J. F. Ziegler, SRIM, Nucl. Instru. Methods Phys. Res. B (2003), **1027**, 219–220, (2004). Available at <http://www.srim.org/>.
- [35] H. Liskien, A. Paulsen, At. Data Nucl. Data Tables **15**, 57 (1975).
- [36] J. W. Meadows, D. L. Smith, National Laboratory Report ANL-7983 (1972).
- [37] C. H. Poppe, J. D. Anderson, J. C. Davis, S. M. Grimes, C. Wong, Phys. Rev. C **14**, 438 (1976).
- [38] NuDat 2.6, National Nuclear Data Center, Brookhaven National Laboratory. Available at: <http://www.nndc.bnl.gov/>(2011).
- [39] P. Andersson, R. Zorro, I. Bergqvist, Conf. On Nucl. Data for Sci. And Technol, K. H. Bockhoff (editor), Antwerp, Belgium, Sept.6-10, Page866, 1982, published by D. Reidel Publishing Company, P. O. Box 17, 3300 A A Dordrecht, Holland.
- [40] H. A. Husain, S. E. Hunt, Int. J. Appl. Radiat. Isot. **34**, 731 (1983).

- [41] P. Andersson, R. Zorro, I. Berqvist, M. Herman, A. Marcinkowski, Nucl. Phys. A **443**, 404 (1985).
- [42] K. I. Zolotarev, P. K. Zolotarev, Progress Report on Research Contract No 16242, INDC (NDS)-0657. Available at <https://www-nds.iaea.org/publications/indc/indc-nds-0657.pdf> (2013).
- [43] R. M. Lindstrom, F. Ronald, R. F. Fleming: Neutron self-shielding factors for simple geometries, revisited. Chem. Anal. (Warsaw) **53**, 855 (2008).
- [44] A. Trkov, G. Zerovnik, L. Snoj, M. Ravnik, Nucl. Instru. Meth. Phys. Res. A **610**, 553 (2009).
- [45] H. Hofmann, J. Richert, J. Tepel, H. Weidenmuller, Ann. Phys. **90**, 403 (1975).
- [46] T. Belgia et al., RIPL-2 Reference input parameter library, IAEA-TECDOC-1506, Vienna. Available at: <http://www-nds.iaea.org/ripl2/> (2006).